Encyclopedia of Quaternary Science, 3rd Edition

Article Title

N_2, O_2, and Ar in ice cores: elemental and isotopic compositions

Author and Co-author Contact Information

Ikumi Oyabu
10-3 Midori-cho, Tachikawa, Tokyo, 190-8518 Japan
oyabu.ikumi@nipr.ac.jp
+81-(0)42-512-0680

Kenji Kawamura
10-3 Midori-cho, Tachikawa, Tokyo, 190-8518 Japan
kawamura@nipr.ac.jp
+81-(0)42-512-0684

Abstract:

The elemental and isotopic ratios of N_2, O_2 and Ar in ice cores provide various paleoenvironmental information on global to local scales, including local summer insolation proxy for Antarctic deep ice-core dating (O_2/N_2), atmospheric O_2 concentration (O_2/N_2), firn thickness ($\delta^{15}N$, $\delta^{40}Ar$), mean surface temperature and abrupt changes ($\delta^{15}N$, $\delta^{40}Ar$), and low latitude hydrological cycle ($\delta^{18}O$). This article provides an overview of the theory, methods and major findings on each component.

Keywords :

Abrupt climate change
Argon
Bubble close-off
Chronology
Clathrate hydrate
Dole effect
Firn thickness
Gas loss
Gravitational fractionation
Hydrological cycle
Nitrogen
Orbital tuning
Summer insolation
Surface temperature
Thermal fractionation

Key points/objectives box:

- $\delta O_2/N_2$ provides a local summer insolation proxy for Antarctic deep ice core dating, and past atmospheric O_2 content over long ($>10^5$-year) timescales.
- $\delta^{15}N$ and $\delta^{40}Ar$ provide gravitational and thermal fractionations by molecular diffusion in firn, and are used to reconstruct past firn thickness and surface temperature.
- $\delta^{18}O_{atm}$ contains information on global ice volume and low-latitude hydrological cycle associated with abrupt climate changes.

Introduction

Air in polar ice sheets provides information on the histories of climate and atmosphere. Atmospheric air is transported through firn (typical thickness: 50 – 100 m) by molecular diffusion, advection and convection, before being trapped as air bubbles. These processes alter the elemental and isotopic ratios of N_2, O_2 and Ar (e.g., mass-dependent gravitational fractionation, thermal separation, and size-dependent close-off fractionation), imprinting the past glaciological and climatological conditions in the gas fractionation signals.

$\delta O_2/N_2$ and $\delta Ar/N_2$ primarily reflect the fractionation during the bubble close-off. In inland Antarctic ice cores, the variations of $\delta O_2/N_2$ are highly correlated with those of local summer insolation at the coring site through physical processes of snow and firn. It has thus been used as a chronological constraint for deep ice cores. It can also be used to reconstruct past atmospheric O_2 variation if the fractionation processes are understood.

Because the atmospheric $\delta^{15}N$ of N_2 is unchanged over the timescales of ice core studies, $\delta^{15}N$ measured in ice cores and firn air reflects physical fractionation processes in firn (mostly gravitational and thermal fractionation due to molecular diffusion). Thus, it can be used to reconstruct past firn thickness and surface temperature changes.

The atmospheric $\delta^{18}O$ of O_2 varies with the changes in global ice volume and low-latitude hydrological cycle, thus $\delta^{18}O$ in ice cores (after correcting for the fractionations acquired in the firn) has been used to reconstruct its atmospheric change in the past to deduce changes in the low-latitude hydrological cycle.

The following sections detail the fractionations of these gases and their applications for various paleoclimatic reconstructions.

$\delta O_2/N_2$ and $\delta Ar/N_2$

Fractionation during bubble close-off

Pioneering studies found that O_2/N_2 and Ar/N_2 in the Camp Century (Greenland) and Byrd (Antarctica) ice cores are lower than the present atmospheric ratios by several %, too low to represent the past atmospheric composition (e.g., Horibe et al., 1985). Subsequent studies confirmed the low O_2 and Ar in many polar ice cores with various glaciological conditions and air inclusions (bubbles or clathrate hydrates), and found that $\delta O_2/N_2$ is generally depleted twice as much as $\delta Ar/N_2$ (Bender et al., 1995; Craig et al., 1988; Sowers et al., 1989). From high-quality ice core measurements, $\delta O_2/N_2$ in the Holocene ice is typically -5 to -10 ‰ with respect to the atmosphere (Vostok core: Bender, 2002; Suwa and Bender, 2008a, Dome Fuji core: Kawamura et al., 2007, Oyabu et al., 2021, GISP2 core: Suwa and Bender, 2008b, Siple Dome core: Severinghaus et al., 2009, EDC core: Bazin et al., 2016; Extier et al., 2018; Landais et al., 2012,WAIS Divide core: Seltzer et al., 2017).

The reason for the low $\delta O_2/N_2$ and $\delta Ar/N_2$ in ice cores is size-dependent fractionation during the bubble close-off process, which preferentially excludes small molecules such as He, Ne, O_2 and Ar from bubbles, and enriching them in the open pores as evident from firn air measurements (Battle et al., 1996; Huber et al., 2006a; Severinghaus and Battle, 2006) (Fig. 1). The mechanism of the gas loss from freshly closed air bubbles is molecular diffusion through the thin ice wall, driven by increasing bubble pressure due to firn densification. The fractionation has an apparent threshold molecular diameter of ~3.6 Å (below which the gases are preferentially excluded from bubbles), which may be related to the size of channels in the ice crystal structure (Huber et al., 2006a). On the other hand, molecular dynamics simulations suggested two types of mechanisms of gas diffusion in ice: the breaking-bond mechanism for relatively large molecules (such as O_2, N_2, CH_4 and CO_2), and the interstitial mechanism for small molecules (Ikeda-Fukazawa et al., 2004). The diffusion coefficients for the bond-breaking mechanism are larger than those from the interstitial mechanism by orders of magnitude, and the value for O_2 is larger than that for Ar, consistent with the larger fractionation for $\delta O_2/N_2$ in the data.

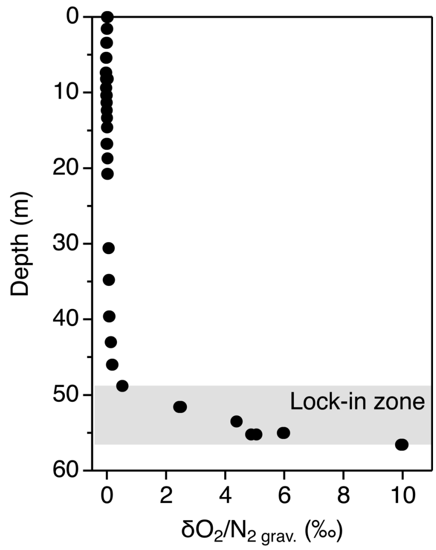

Figure 1: Depth profile of $\delta O_2/N_2$ in firn at Siple Dome (Severinghaus et al., 2001). Note the significant enrichment in the lock-in zone, indicating preferential O_2 loss from the air bubbles (and resulting enrichment in the open pores of the lock-in zone).

Fractionation between bubbles and clathrate hydrates

In the polar ice sheets, air bubbles are compressed with depth in accordance with the increasing overburden pressure. When the pressure exceeds a certain level, the air bubbles cannot stably exist and they gradually transform into clathrate hydrates (also called air hydrates, or clathrates). In the bubble-clathrate transition zone (BCTZ), extreme gas fractionations occur between bubbles and clathrate hydrates (e.g., Ikeda-Fukazawa et al., 2001). Depending on the ice temperature, the BCTZ starts at ~450 – 1000 m and ends at ~1200 – 1500 m (deeper for warmer sites) (Uchida et al., 2014). Raman spectroscopic measurements of individual air inclusions found that O_2 is enriched in clathrate hydrates in the BCTZ (Ikeda et al., 1999; Ikeda-Fukazawa et al., 2001). In the Vostok and Dome Fuji ice cores, they found that $\delta O_2/N_2$ in air bubbles decreases with depth from ~0 ‰ to extremely negative values (~ -740 ‰). On the other hand, the clathrate hydrates is extremely enriched in O_2 (> +1000 ‰) in the upper part of BCTZ, and gradually decrease towards ~0 ‰ at the bottom of BCTZ (Fig. 2, Ikeda et al., 1999 and Ikeda-Fukazawa et al., 2001). The extreme $\delta O_2/N_2$ fractionation between the coexisting bubbles and clathrate hydrates (Fig. 2) may be due to lower dissociation pressure and larger permeation coefficient of O_2 relative to N_2 (e.g., Ikeda-Fukazawa et al., 2001).

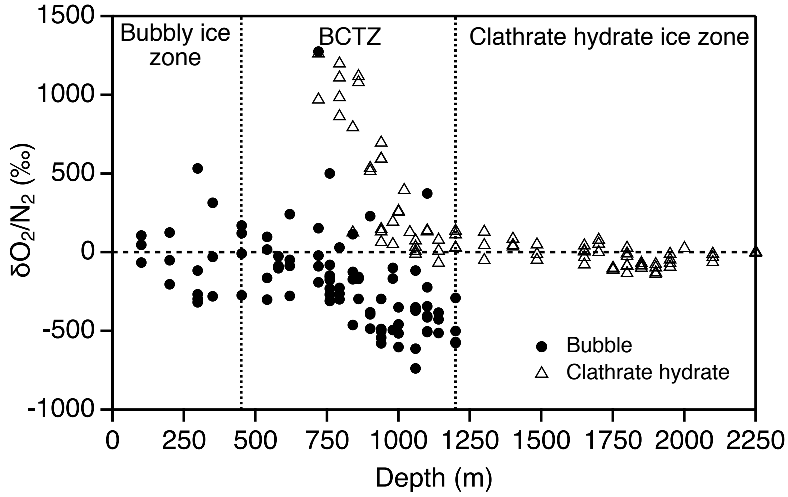

Figure 2: $\delta O_2/N_2$ in individual air bubbles and clathrate hydrates in the Dome Fuji ice core observed by Raman spectroscopy (Ikeda-Fukazawa et al., 2001). Extremely large fractionation between bubbles and clathrates in the BCTZ is observed.

The gas fractionations on individual bubbles and clathrates probably cause the very high variabilities in $\delta O_2/N_2$ and $\delta Ar/N_2$ of bulk ice samples (Bender, 2002; Kawamura et al., 2007; Kobashi et al., 2008b; Oyabu et al., 2021) (Fig. 3). The bubbles and clathrate hydrates are concentrated in mm-scale layers (Ohno et al., 2010), thus any ice sample may randomly include the fractionated layers and bring the scatter in the $\delta O_2/N_2$ and $\delta Ar/N_2$ data (Oyabu et al., 2021). Thus, it may be possible to reduce the scatters by measuring much longer samples (Lüthi et al., 2010; Oyabu et al., 2021; Shackleton et al., 2019).

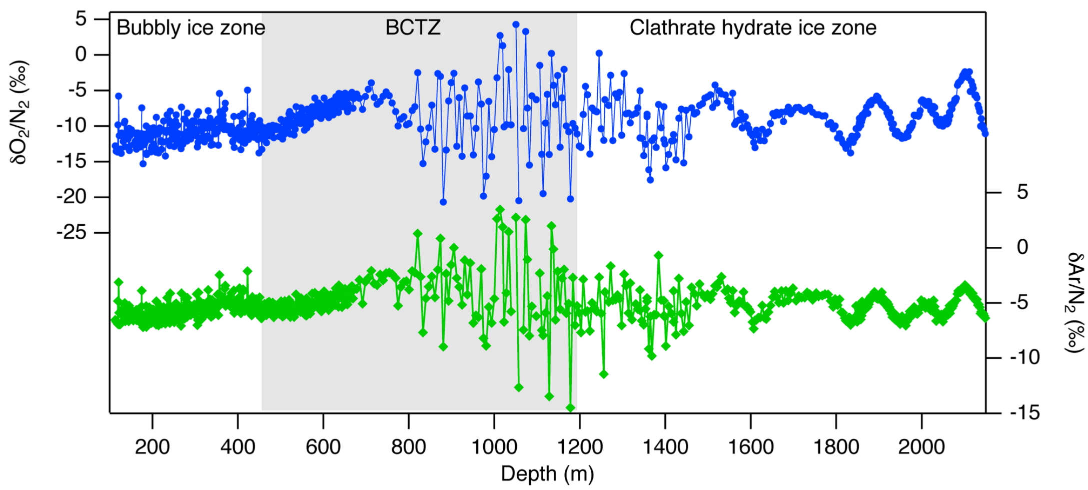

Figure 3: $\delta O_2/N_2$ and $\delta Ar/N_2$ of bulk ice samples (~12 cm long) of the Dome Fuji core (Oyabu et al., 2021). Note the large scatter in the lower half of the BCTZ, which may be the artifact of the combination of microscopic fractionation and finite sample length.

Homogenization below the BCTZ

Below the BCTZ, the scatter in $\delta O_2/N_2$ and $\delta Ar/N_2$ data decreases with depth over several hundred meters (Bender, 2002; Shackleton et al., 2019; Oyabu et al., 2021) (Fig. 3). For example, the Dome Fuji core shows large scatter until ~1500 m, whose age is ~25 kyr older than the bottom of BCTZ. This is probably the remnant of the fractionation in the BCTZ, which is slowly homogenized by a diffusive process. One-dimensional diffusion models (Oyabu et al., 2021) can simulate the observed homogenization with a published set of gas permeation coefficients (Salamatin et al., 2001).

Artifactual gas-loss fractionation

Fractionation of relatively small gas molecules (e.g. H_2, Ne, O_2 and Ar) also occurs by gas loss during ice-core drilling and storage, which depletes $\delta O_2/N_2$ and $\delta Ar/N_2$ while enriching $\delta^{18}O$ and $\delta^{40}Ar$ (Bender et al., 1995; Craig et al., 1988; Ikeda-Fukazawa et al., 2005; Kawamura et al., 2007; Kobashi et al., 2008b; Oyabu et al., 2020; Oyabu et al., 2021; Severinghaus et al., 2009; Sowers et al., 1989). The fractionation is caused by gas loss through microcracks (Bender et al., 1995) and diffusion through the ice (Ikeda-Fukazawa et al., 2005). Ice cores stored in ordinary cold storage (-25 – -35 °C) show significant $\delta O_2/N_2$ depletion over months to years (Kawamura et al., 2007; Suwa and Bender, 2008a, b). Gas loss may also fractionate the isotopic ratios of O_2 and Ar, which require appropriate corrections (Landais et al., 2010; Severinghaus et al., 2009). For example, $\delta^{18}O$ from the Siple Dome core was corrected for gas loss using a large dataset of paired differences of $\delta^{18}O$, $\delta O_2/N_2$ and $\delta Ar/N_2$ from duplicate measurements (Severinghaus et al., 2009).

If ice samples are stored at a much lower temperature (-50 °C), the diffusive gas loss is significantly reduced, and numerical models suggest that the gas-loss fractionation over a few decades may be limited to <~10 mm from the sample surface (Ikeda-Fukazawa et al., 2005). Indeed, the measurements on the Dome Fuji core found the original $\delta O_2/N_2$ in the inner part of the ice samples that had been stored at -50 ˚C for ~20 years (Oyabu et al., 2020, 2021).

Local summer insolation proxy for ice core dating

The variations of $\delta O_2/N_2$ for inland Antarctic ice cores are highly correlated with those of local summer insolation on orbital timescales (Vostok, Dome Fuji, and Dome C) (Bender, 2002; Kawamura et al., 2007; Oyabu et al., 2021; Extier et al., 2018). Summer insolation varies by >20 % on precessional cycles (~23 kyr periods), which varies the magnitude of snow metamorphism in near-surface firn. The contrasts in physical properties are retained through firn densification and influence the magnitude of the gas fractionations during bubble close-off (Bender, 2002; Fujita et al., 2009; Kawamura et al., 2007). Because of the large scatter in the $\delta O_2/N_2$ records in the BCTZ (see above), a clear insolation signal is only visible below the BCTZ (Bender, 2002; Extier et al., 2018; Oyabu et al., 2022) (Fig. 4).

Using the close similarity of $\delta O_2/N_2$ with insolation, the $\delta O_2/N_2$ has been used to orbitally tune Antarctic ice cores (Bazin et al., 2013; Kawamura et al., 2007; Oyabu et al., 2022; Suwa and Bender, 2008a) (Fig. 4). If $\delta O_2/N_2$ records the insolation variations without significant climatic signals, it provides a rare opportunity to study the phasing between orbital parameters and climate (Kawamura et al., 2007; Suwa and Bender, 2008a). Recent $\delta O_2/N_2$ data from the Dome Fuji core between 90 – 200 kyr BP, which are free from the artifactual gas-loss fractionation, suggest negligible phasing between $\delta O_2/N_2$ and local summer solstice insolation (Oyabu et al., 2022). Note that the EDC $\delta O_2/N_2$ record shows a 100-kyr periodicity between 340 and 800 kyr BP (Bazin et al., 2016; Landais et al., 2012), suggesting some climatic influence on that core.

Note that temperature and accumulation rate should also affect the firn metamorphism and $\delta O_2/N_2$ fractionation. For example, $\delta O_2/N_2$ in the GISP2 ice core, Greenland, correlates with both local summer insolation (on orbital timescales) and water isotope ratios (on millennial timescales), suggesting the influence of accumulation changes on the close-off fractionation (Suwa and Bender, 2008b). In the Antarctic inland cores, $\delta O_2/N_2$ records show negligible 100-kyr periodicity (the largest climatic signal), possibly because the effects of temperature and accumulation cancel out (Hutterli et al., 2009; Kawamura et al., 2007).

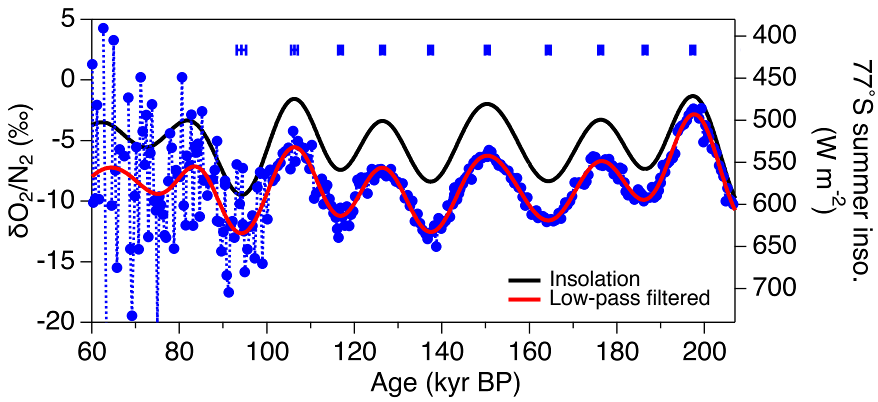

Figure 4: $\delta O_2/N_2$ data of the Dome Fuji core and summer solstice insolation at 77 ˚S (Oyabu et al., 2022). Blue markers with error bars at the top indicate age markers for DF2021 chronology with 2σ uncertainty. Note that the large scatter for the youngest part is caused by bubble-clathrate transformation (see “Fractionation between bubbles and clathrate hydrates”).

Past atmospheric O_2 concentration

Reconstruction of past atmospheric $\delta O_2/N_2$ from the ice core data is challenging because of the bubble close-off fractionation and artifactual gas-loss fractionation, whose variations may overwhelm the atmospheric signal. However, the atmospheric $\delta O_2/N_2$ trend over very long timescales has been constrained by combining multiple ice core records, which suggest -8.4 ± 0.2 ‰ per million years over the last 800 kyr (Extier et al., 2018; Landais et al., 2012; Stolper et al., 2016) (Fig. 5). It is interpreted as a decrease in atmospheric O_2 concentration because the lifetime of atmospheric N_2 is about a billion years (Berner, 2006). The O_2 decrease might be caused by changes in burial and weathering fluxes of organic carbon and pyrite, driven by Neogene cooling or increasing Pleistocene erosion rates (Stolper et al., 2016). More recently, discontinuous ice samples from the Allan Hills blue ice area revealed that the atmospheric $\delta O_2/N_2$ at ~1.5 Myr was similar to the value at

810 kyr BP (Fig. 5), suggesting that the imbalance between O_2 sources and sinks began around 800 kyr BP, perhaps in relation to the development of the 100-kyr glacial cycles (Yan et al. (2021).

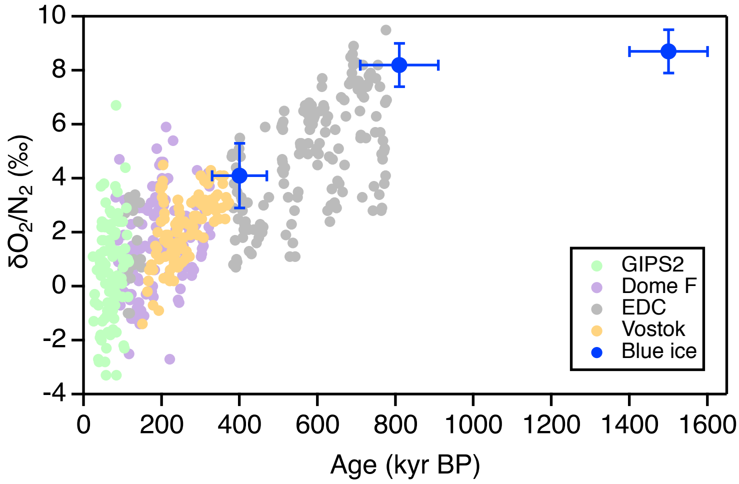

Figure 5: Atmospheric $\delta O_2/N_2$ from GISP2, Dome Fuji, EDC and Vostok ice cores (Stolper et al., 2016) and Allan Hills blue ice (Yan et al., 2021).

$\delta^{15}N$ of N_2

Gravitational and thermal fractionation in firn

Because of the long lifetime of atmospheric N_2 (a billion-year timescale, Berner, 2006), $\delta^{15}N$ of N_2 is thought to be stable in the atmosphere. Thus, $\delta^{15}N$ measured in ice cores and firn air, which are non-zero, reflect fractionations in the firn column associated with gas transport processes (e.g., molecular diffusion and convection). Firn is schematically divided into three zones in terms of gas transport (Sowers et al., 1992): convective zone, diffusive zone and lock-in zone from top to bottom (Fig. 6). In the convective zone, the firn air is mixed well with the overlying atmosphere over the timescales of a year or longer. In the lock-in zone, $\delta^{15}N$ is almost constant because the molecular diffusion becomes very small.

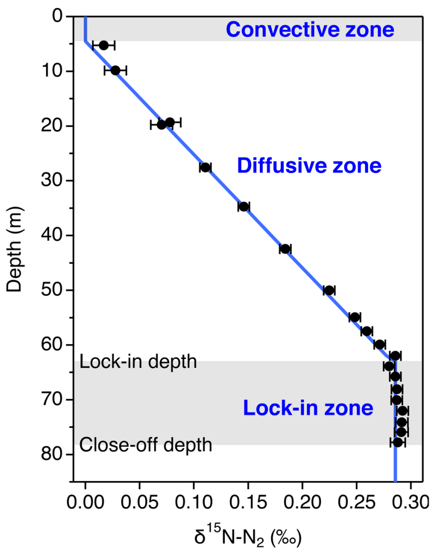

Figure 6: Different zones in firn in terms of gas transport, and their effects on gravitational enrichment of $\delta^{15}N$ (after correction for thermal fractionation) (Buizert et al., 2012)

In the diffusive zone, molecular diffusion dominates the gas movement; thus, gravitational and thermal fractionations occur. Gravitational fractionation is described by the barometric equation (Craig et al., 1988; Sowers et al., 1989):

$$\delta_{grav} = \left(\exp\left(\frac{\Delta mgz}{RT}\right) - 1\right) \cdot 1000\ (‰) \cong \frac{\Delta mgz}{RT} \cdot 1000\ (‰) \qquad (1)$$

where Δm is the mass difference between the isotope pair (kg mol^{-1}), g is the acceleration of gravity, z is the thickness of the diffusive zone, R is gas constant, and T is temperature (K).

The thermal fractionation occurs under a temperature gradient in the firn column such that the heavier gases are concentrated at the cold end (Severinghaus et al., 1998). The temperature profile of the firn column is largely determined by the downward advection of ice and upward conduction of geothermal heat. The magnitude of the fractionation is given by

$$\delta_{therm} = \Omega \cdot \Delta T \qquad (2)$$

where Ω is gas-specific thermal diffusion sensitivity (‰ K^{-1}), and ΔT is the temperature difference between the top and bottom of the diffusive zone, respectively. Ω is experimentally determined by equilibrating an air sample in a known temperature gradient and measuring the steady-state fractionation (Grachev and Severinghaus, 2003a, b; Kawamura et al., 2013; Severinghaus and Brook, 1999). It is also dependent on the mean temperature and typically given by:

$$\Omega = \frac{a}{T_{av}} - \frac{b}{T_{av}^2} \qquad (3)$$

where a and b are constants constrained by the data (Table 1) and T_{av} is the effective average temperature. The effective average temperature is

$$T_{av} = \frac{T_{cold}T_{hot}}{T_{hot} - T_{cold}} \ln\left(\frac{T_{hot}}{T_{cold}}\right). \qquad (4)$$

Thus, the measured $\delta^{15}N$ can be expressed as

$$\delta^{15}N_{measured} = \delta^{15}N_{grav} + \delta^{15}N_{therm}$$

$$= \frac{gz}{RT} + \Omega^{15/14}\,\Delta T \qquad (5)$$

Similarly, measured $\delta^{40}Ar$ can be expressed as

$$\delta^{40}Ar_{measured} = \delta^{40}Ar_{grav} + \delta^{40}Ar_{therm}$$

$$= 4\frac{gz}{RT} + \Omega^{40/36}\ \Delta T \qquad (6)$$

The gravitational and thermal components can be separated by combining eqs. (5) and (6). The temperature gradient in firn can thus be obtained by the difference between the measured $\delta^{15}N$ and $\delta^{40}Ar$ (called $\delta^{15}N_{excess}$):

$$\delta^{15}N_{excess} = \delta^{15}N_{measured} - \frac{1}{4}\delta^{40}Ar_{measured}$$

$$= \left(\Omega^{15/14} - \frac{1}{4}\Omega^{40/36}\right)\ \Delta T \tag{7}$$

$$\Delta T = \frac{\delta^{15}N_{excess}}{\left(\Omega^{15/14} - \frac{1}{4}\Omega^{40/36}\right)} \tag{8}$$

Table 1: Thermal diffusion sensitivity, $\Omega = a/T - b/T^2$.

Gas pair	Thermal diffusion sensitivity Ω (‰ K^{-1})		Ω at -30˚C
	a	*b*	
$^{15}N^{14}N/^{28}N_2$	8.656[1]	1232[1]	0.0148
$^{40}Ar/^{36}Ar$	26.08[2]	3952[2]	0.0404
$^{86}Kr/^{82}Kr$	5.05[3]	580[3]	0.0110
$^{136}Xe/^{132}Xe$	11.07[3]	2000[3]	0.0117

[1] Grachev and Severinghaus (2003b)
[2] Grachev and Severinghaus (2003a)
[3] Kawamura et al. (2013)

Two methods are available for obtaining $\delta^{15}N$ and $\delta^{40}Ar$ at the same depth: (1) using separate ice samples for $\delta^{15}N$ and $\delta^{40}Ar$ and (2) using a single sample for both species. In the former method, $\delta^{15}N$ is measured on a relatively small sample (~10 to 50 g) after removing CO_2 from the extracted air (e.g., Oyabu et al., 2020), and $\delta^{40}Ar$ is measured on a larger sample (~100 g) after removing all reactive gases in the air sample with a process called gettering, leaving only noble gases (e.g., (Severinghaus et al., 2003). The noble gas sample is mixed with pure nitrogen to have enough pressure for mass spectrometry. In the latter method, O_2 is removed from extracted air with heated copper (Kobashi et al., 2008b; Morgan et al., 2022). It is more advantageous than the first method for temperature reconstruction because any mass-dependent fractionations (both natural and experimental) affect $\delta^{15}N$ and $\delta^{40}Ar/4$ with the same magnitude, and thus can be precisely canceled out in eq. 7.

Past firn thickness

In the absence of rapid temperature changes, $\delta^{15}N$ and $\delta^{40}Ar$ in ice cores mostly reflect the gravitational fractionation in the diffusive zone (Schwander et al., 1997; Sowers et al., 1992). Thus, they are the indicators of past firn thickness. The ice cores from Greenland (GRIP, NGRIP, GISP2) and Antarctica (Byrd and WAIS Divide) show smaller $\delta^{15}N$ in the Holocene than in the last glacial period, suggesting that firn was thicker in the glacial period at those sites. The smaller firn in warmer periods is consistent with the modern spatial relationship between the temperature and firn thickness, and also the predicted changes in firn thickness by firn densification models. On the other hand, in the inland of East Antarctica (Vostok, Dome C, Dome Fuji, EDML), $\delta^{15}N$ are larger in the interglacial periods than in the glacial periods, which appear contradictory to the prediction of classic densification models as well as the modern spatial relationship between the temperature and firn thickness (Landais et al., 2006) (Fig. 7).

Several hypotheses have been proposed for explaining the discrepancy between the gas data and firn models; (1) the convective zones were thicker in the glacial periods, (2) the dependence of densification rate on temperature and accumulation rate is not appropriate for the glacial climate in East Antarctica (note that the models cannot be calibrated with the glacial conditions for those sites (much colder and drier conditions), or (3) the input for the models (glacial temperature and/or accumulation rate) is incorrect.

To reconcile the discrepancy between the smaller diffusive zone from data and larger firn thickness in the models in the glacial periods, the required convective zone thickness in the East Antarctic inland is up to ~40 m (e.g., Sowers et al., 1992). From modern observations, the deepest convective zone is 23 m, which was found at an ultralow-accumulation site in the Megadunes area in central Antarctica (Severinghaus et al., 2010). The second deepest convective zone of 14 m is found at YM85 in Dronning Maud Land, in a strong katabatic wind region with a mean wind speed of $\sim$12 m s^{-1} (Kawamura et al., 2006). The possibility of deeper convective zones during the glacial periods cannot be ruled out, but it seems rather unlikely that such deep convection was developed at Dome C and Dome Fuji from the chronological constraints, as follows.

The past firn thickness can be estimated from the depth difference between ice and gas for the same age (Δdepth) divided by thinning function and mean firn density relative to the ice density (~0.7). The Δdepth is constrained by synchronizing the ice age and gas age to those of other well-dated ice cores (e.g., WAIS Divide core), and the thinning is estimated with a 1-D ice flow model. The method is limited to the last 50 kyr because of the requirements of well-dated ice cores and small uncertainty in the thinning, and the resulting firn thickness from the LGM to the last termination is consistent with the diffusive column height from the $\delta^{15}N$ data (Oyabu et al., 2022; Parrenin et al., 2012). More direct estimation using isotopic ratios of three gases (N_2, Ar and a heavy noble gas) in the ice cores is awaited (Kawamura et al., 2013).

The lack of very thick convective zone (i.e., thinner firn) in the last glacial period suggests an overestimation of the modeled firn thickness, either by a flaw in the models or the input data to drive them (Fig. 7). Recent studies have reduced the mismatch between the modeled and $\delta^{15}N$-based firn thickness in East Antarctica. On the one hand, the firn densification model with modified sensitivity to temperature as well as softening of firn by impurities enhances the densification rates in the glacial periods (Bréant et al., 2017). The model reproduces thinner firn in the glacial climate at Dome C, Vostok and Dome Fuji, but the same parameterization (with dust effect) underestimates the glacial-interglacial firn thickness changes at higher accumulation sites (WAIS Divide and NGRIP) (Bréant et al., 2017; Oyabu et al., 2022). On the other hand, the traditional firn models may reproduce thinner glacial firn if the glacial surface temperature was warmer than the traditional estimates. Inversion of the traditional densification models for temperature and accumulation rate constrained by the $\delta^{15}N$ and Δage data found ~4 ˚C cooling in East Antarctic inland during the LGM (vs. today), much warmer than the classic stable water isotope thermometry (~9 ˚C, Jouzel et al., 2007) (see below).

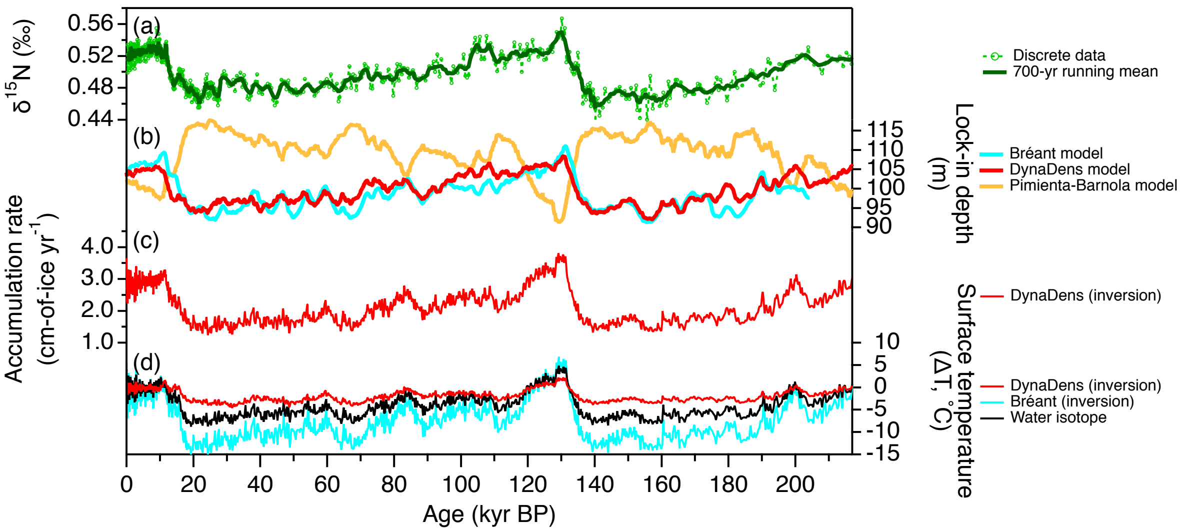

Figure 7: Time series of $\delta^{15}N$ data and model-derived parameters for the Dome Fuji core (Oyabu et al., 2022). (a) $\delta^{15}N$ data, (b) lock-in depth from model inversions constrained by $\delta^{15}N$ (red and blue) and forward modeling with 9 ˚C cooling in the LGM (yellow), (c) accumulation rate from model inversion, and (d) surface temperature from DynaDens model inversion (red), Bréant model inversion (blue), and water isotope thermometry (black, Uemura et al., 2018).

Temperature reconstruction

In Greenland ice cores, rapid surface temperature changes are recorded as anomalies of $\delta^{15}N$ and $\delta^{40}Ar$ with respect to the gravitational signals, caused by thermal diffusion in firn (see above). Because gas diffusion is ~10 times faster than heat diffusion (Paterson, 1969), the thermal fractionation of gases occurs between the top and bottom of the firn, and the signal is locked in air bubbles before the temperature of the whole firn equilibrates. The gas isotope data and firn models may be combined to reconstruct the surface temperature evolution. Earlier studies employed forward firn modeling to find the magnitude of step-wise surface warming (e.g., Severinghaus and Brook, 1999; Severinghaus et al., 1998) (Fig. 8) or the scaling factor of $\delta^{18}O_{ice}$ to temperature (e.g., (Landais et al., 2004; Lang et al., 1999) for each abrupt event. If only $\delta^{15}N$ data is available, $\delta^{15}N_{grav}$ and $\delta^{15}N_{therm}$ are separated with a firn densification model with heat transfer (Huber et al., 2006b; Buizert et al., 2014). More advanced inversion techniques are employed in later studies to continuously reconstruct the surface temperature history over multiple abrupt changes and relatively stable periods (Buizert et al., 2014; Huber et al., 2006b; Kobashi et al., 2008a; Orsi et al., 2014).

The abrupt climate changes in the gas records also provide chronological constraints on (1) the relative timing of surface temperature and greenhouse gas changes, and (2) Δage by comparing $\delta^{15}N$ with $\delta^{18}O_{ice}$ for the same event. For the abrupt climate changes during the last glacial period and deglaciation, Greenland surface warmings preceded the CH_4 changes by ~20 – 30 years (Severinghaus and Brook 1999) (Fig. 8).

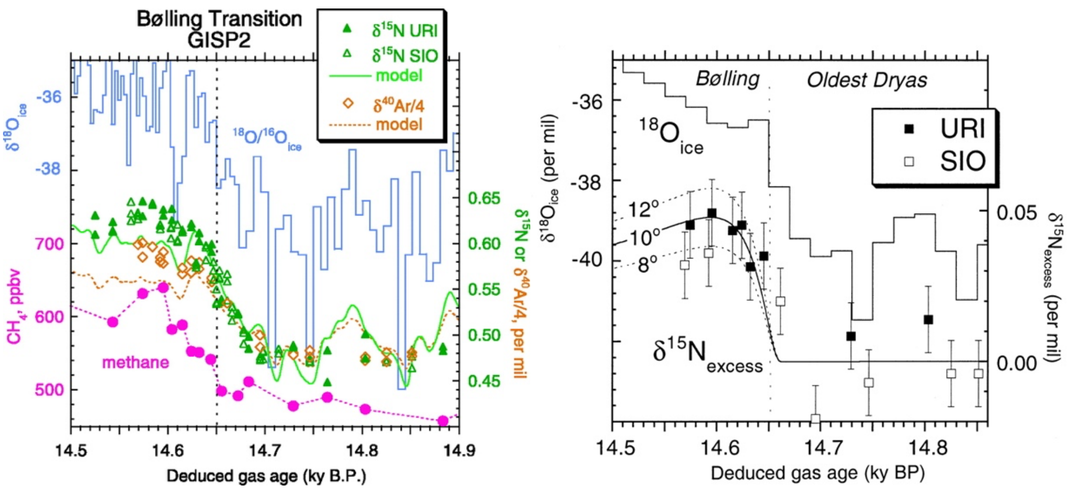

Figure 8: $\delta^{18}O_{ice}$, $\delta^{15}N$, $\delta^{40}Ar/4$ and CH_4 data (left) and $\delta^{15}N_{excess}$ (right) of the GISP2 core at the Bølling transition (from Severinghaus and Brook, 1999; reproduced with permission).

Based on the earlier $\delta^{15}N$ studies on the abrupt transitions, Buizert et al. (2014, 2021) developed an automated inversion method of firn densification models to find the best temperature and accumulation history that optimize the modeled $\delta^{15}N$ and Δage to fit with the data. The method allowed to reconstruct both the abrupt changes and long-term variations for three sites from the summit to northwest Greenland (Buizert et al., 2014). The abrupt changes are larger in central Greenland (9° to 14°C) than in northwest Greenland (5° to 9°C), suggesting a North Atlantic origin for the abrupt changes (Fig. 9). The Younger Dryas period was 4.5° to 2°C warmer than the Oldest Dryas (due to increased CO_2 and insolation forcings), contrary to $\delta^{18}O_{ice}$ that are lower in the Younger Dryas (suggesting changing seasonal bias for $\delta^{18}O_{ice}$) (Fig. 9).

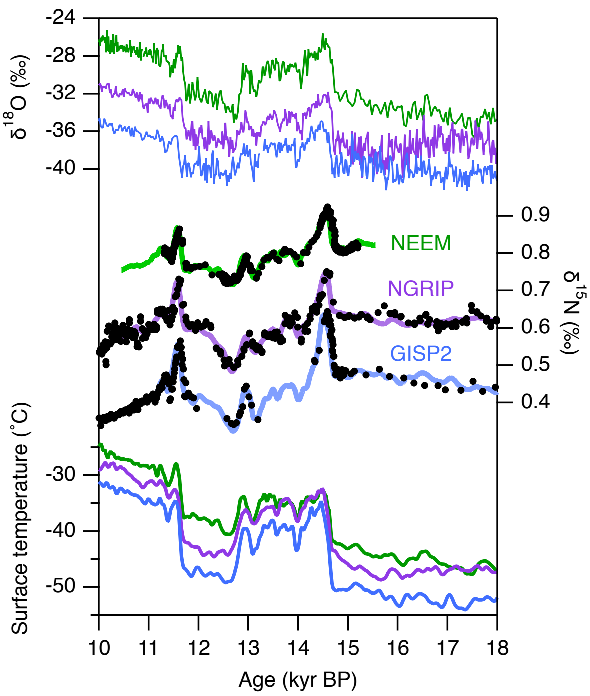

Figure 9: Greenland temperature reconstructions for the last deglaciation (Buizert et al., 2014). (a) Stable water isotope ratios from NEEM (green, offset by +8‰ for clarity), NGRIP (purple, offset by

+4‰) and GISP2 (blue). (b) $\delta^{15}N$ data (black dots) and model results of NEEM (green, offset by +0.4‰), NGRIP (purple, 0.2‰ offset) and GISP2 (blue). (c) Greenland temperature reconstructions for NEEM (green, offset by +6˚C), NGRIP (purple, offset by +3˚C) and GISP2 (blue).

For Antarctica, the recent progress on high-resolution $\delta^{15}N$ and empirical Δage allowed the application of the firn-model inversion to seven sites with vastly different climates (Buizert et al., 2021). They estimated that the LGM temperatures were -4.3±1.5°C at Dome C and -3.8±2°C at Dome Fuji with respect to the late Holocene, which are warmer than the estimates with stable water isotopes (~-9°C). These results are consistent with the independent estimates based on the inversion of an ice sheet model with heat transfer constrained by borehole temperature and vertical ice velocity (Buizert et al., 2021). The LGM cooling was much larger in West Antarctica; e.g., -10.3±1.3°C at WAIS Divide and -10.2±2.4°C at Siple Dome, possibly due to their higher surface elevation in the LGM. Note that the firn-model-based temperature reconstruction for East Antarctica is inconsistent with the latest water isotope thermometry (Markle and Steig, 2022). Thus, the past East Antarctic temperature is a subject of continuing debate.

It was recently found that $\delta^{15}N_{therm}$ in the South Pole and Dome Fuji cores contain seasonal bias due to preferential preservation of winter $\delta^{15}N_{therm}$ anomaly created in the upper firn (Morgan et al., 2022). Their impacts on the paleoclimatic reconstructions are yet to be explored, but it may be significant if the bias changes over time (e.g., glacial vs. interglacial). Careful assessments of rectification at various sites would be necessary for the accurate interpretation of gas isotope thermometry data from Antarctic ice cores.

$\delta^{18}O$ of O_2

Temporal changes in $\delta^{18}O_{atm}$ and the Dole effect

The $\delta^{18}O$ of O_2 in the atmosphere ($\delta^{18}O_{atm}$) may be reconstructed from the measured $\delta^{18}O$ corrected for gravitational enrichment using $\delta^{15}N$ ($\delta^{18}O_{atm} = \delta^{18}O - 2\times\delta^{15}N$). Artefactual enrichment of $\delta^{18}O$ in ice cores may occur by post-coring gas loss, and the correction is necessary for precise $\delta^{18}O_{atm}$ reconstructions (e.g., Landais et al., 2010; Severinghaus et al., 2009). The $\delta^{18}O$ may also be fractionated during bubble close-off as revealed by a firn air study at WAIS Divide (Battle et al., 2011), although no evidence has been found from ice core studies (thus, no correction is applied).

The $\delta^{18}O_{atm}$ varies in response to the growth and decay of the ice sheet (through the changes in oceanic $\delta^{18}O$) and the changes in the $\delta^{18}O$ fractionation between ocean and atmosphere (via respiration and photosynthesis by the marine and terrestrial biosphere). The turnover time of O_2 in the atmosphere is about 1 kyr (Bender et al., 1994), thus, the ice cores from Antarctica and Greenland should record the same atmospheric signals. The dominant periodicities in the $\delta^{18}O_{atm}$ variations are ~23 kyr (precession band) and ~100 kyr (Extier et al., 2018; Jouzel et al., 2002; Kawamura et al., 2007) (Fig. 10).

The $\delta^{18}O_{atm}$ is heavier than $\delta^{18}O$ of the mean ocean by 23.88 ‰ at present (Barkan and Luz, 2005). This enrichment is known as the Dole effect (or Morita-Dole effect) (Dole, 1935; Morita, 1935), most of which is due to the isotopic discrimination by marine and terrestrial respiration preferentially using lighter O_2 (~19 ‰, Bender et al., 1994; Luz and Barkan, 2011). In terms of terrestrial photosynthesis, $\delta^{18}O$ of produced O_2 is similar to that of chloroplast water (e.g., Helman et al., 2005), which, in turn, is enriched relative to soil water due to transpiration. The soil water originates in precipitation, which is depleted in ^{18}O relative to seawater. The net effect of land photosynthesis positively contributes to the Dole effect. The O_2 produced by marine phytoplankton is isotopically enriched relative to ambient seawater (Luz and Barkan, 2011). The marine and terrestrial contributions to the Dole effect are of similar magnitudes (Huang et al., 2020; Luz and Barkan, 2011).

The past changes in the Dole effect may be deduced by subtracting the $\delta^{18}O$ of seawater (estimated from marine sediment cores) from the $\delta^{18}O_{atm}$ (from ice cores). The Dole effect over the last 800 kyr ranges from -0.9 to +0.6 per mil relative to the present value (e.g., Huang et al., 2020). For the seawater $\delta^{18}O$, the global mean $\delta^{18}O$ (i.e., sea-level component) deduced from the benthic foraminiferal $\delta^{18}O$ have typically been used, which shows ~100-kyr and ~23-kyr periodicities as the strongest cycles. On the other hand, a recent study suggested that the Dole effect may better be represented by using the globally stacked sea surface $\delta^{18}O$ instead of $\delta^{18}O$ of the whole ocean (Huang et al., 2020). The newly estimated Dole effect with the sea surface $\delta^{18}O$ contains strong precession cycles (~23 and ~19 kyr) and weak obliquity cycles, but no ~100-kyr cycles. This suggests that the 100-kyr periodicity in the prior estimates may be an artifact, and the temporal changes in the Dole effect may dominantly be controlled by the dynamics of the low-latitude hydrological cycle (Huang et al., 2020). The major role of the low-latitude hydrological cycle on the Dole effect has also been suggested from high-resolution ice core records (Severinghaus et al., 2009), isotope-enabled general circulation models (Reutenauer et al., 2015) and the analyses of modern-day productivity-weighted $\delta^{18}O$ of terrestrial precipitation (Seltzer et al., 2017).

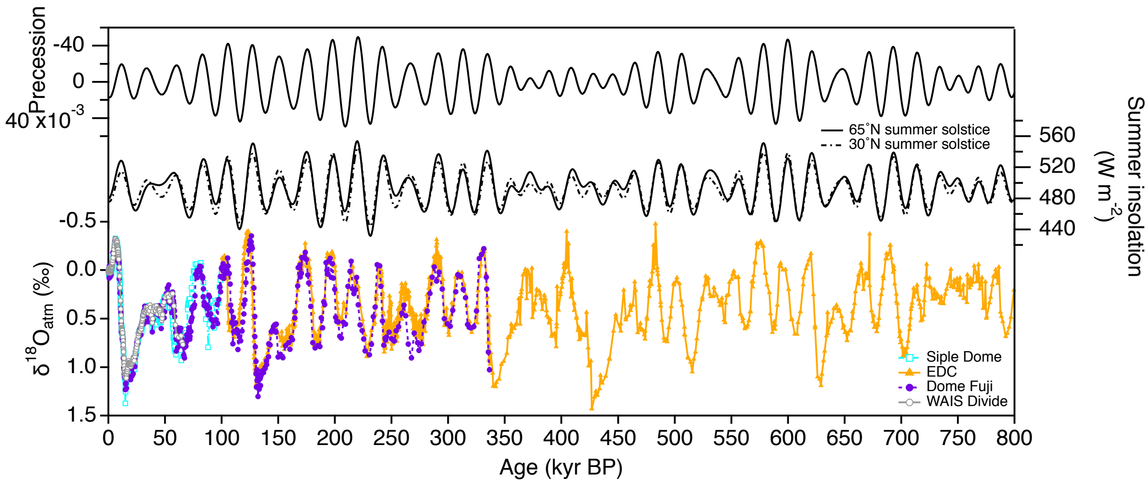

Figure 10: $\delta^{18}O_{atm}$ from Siple Dome (Severinghaus et al., 2009), EDC (Extier et al., 2018), Dome Fuji (Kawamura et al., 2007; Oyabu et al., 2021), and WAIS Divide (Seltzer et al., 2017) cores. Precession parameter and summer insolation at 30N˚ and 65N˚ are also shown.

Tracer of hydrological cycle for abrupt climate changes

Despite the long turnover time of O_2 (~1 kyr), rapid changes of $\delta^{18}O_{atm}$ corresponding to the Dansgaard-Oeschger (DO) events can be identified in high-resolution records (Landais et al., 2007).

The globally integrated $\delta^{18}O$ anomaly (relative to the atmosphere at the time) associated with the terrestrial (hydrological and respiratory) fractionations may be represented by a single parameter $\Delta\varepsilon_{LAND}$ following the equation:

$$\Delta\varepsilon_{LAND} = \left[\tau \frac{d\delta^{18}O_{atm}}{dt} + \delta^{18}O_{atm} - \delta^{18}O_{seawater}\right]\frac{1}{f_L} \qquad (9)$$

where τ is the turnover time of 1000 years, f_L is the fraction of photosynthesis occurring on land (assumed to be 0.65), $\delta^{18}O_{atm}$ is $\delta^{18}O$ of atmospheric O_2 relative to the modern atmosphere, and $\delta^{18}O_{seawater}$ is $\delta^{18}O$ of seawater relative to the modern value (i.e., SMOW). Note the underlying assumptions that oceanic photosynthesis produces no fractionation relative to seawater, that the temporal variation in the oceanic respiratory fractionation is negligible, and that the fraction of total oxygenases on land (f_L) is constant over time. The first and second terms in the right-hand side of the equation are constrained by the ice-core data, and the third term is constrained by paleoceanographic data. In summary, "if respiratory fractionation is constant, $\Delta\varepsilon_{LAND}$ would be equal to the isotopic fractionation of terrestrial chloroplast water relative to seawater. In this case, $\Delta\varepsilon_{LAND}$ would give globally integrated information about the hydrological cycle, in particular, the $\delta^{18}O$ of precipitation over photosynthetically active land areas such as the monsoon regions, and the relative humidity in these areas" (Severinghaus et al., 2009).

The modern seasonal cycle of $\delta^{18}O$ of terrestrial precipitation weighted by gross primary productivity (GPP) (i.e., mean $\delta^{18}O$ of source water for O_2 production) negatively correlates with the centroid latitude of terrestrial oxygen production (Seltzer et al., 2017). This relationship suggests that a positive $\delta^{18}O_{atm}$ (or $\Delta\varepsilon_{LAND}$) anomaly in the past is associated with a southward shift of ITCZ. The $\Delta\varepsilon_{LAND}$ from the Siple Dome and WAIS Divide cores for the last 50 kyr BP shows significant positive correlations with the Chinese speleothem $\delta^{18}O$ records (indicators of monsoon strength) (Severinghaus et al., 2009; Seltzer et al., 2017) (Fig. 11). The $\Delta\varepsilon_{LAND}$ rapidly becomes lighter synchronously with the DO warmings and vice versa during the DO cooling. In addition, $\Delta\varepsilon_{LAND}$ shows abrupt and strong increases during the Heinrich Stadials (stadial periods including massive iceberg discharge events into the North Atlantic known as Heinrich Events), and the maxima in $\Delta\varepsilon_{LAND}$ are synchronous with or shortly after the relatively small CH_4 peaks within the Heinrich Stadials (Rhodes et al., 2015). The Heinrich Events shut down the Atlantic meridional overturning circulation (e.g., Oppo and Lehman, 1995), which forced the ITCZ to occupy an extreme southerly location and intensified southern tropical precipitation, increasing the southern CH_4 emission and $\delta^{18}O_{atm}$.

The reconstruction of $\Delta\varepsilon_{LAND}$ on longer time scales remains a challenge. The $\Delta\varepsilon_{LAND}$ over multiple glacial cycles from the EDC core does not resemble the variations of Chinese speleothem $\delta^{18}O$, possibly because of the relative chronological uncertainty of $\delta^{18}O_{seawater}$ relative to $\delta^{18}O_{atm}$ (Extier et al., 2018) as well as the choice of $\delta^{18}O_{seawater}$ (Huang et al., 2020).

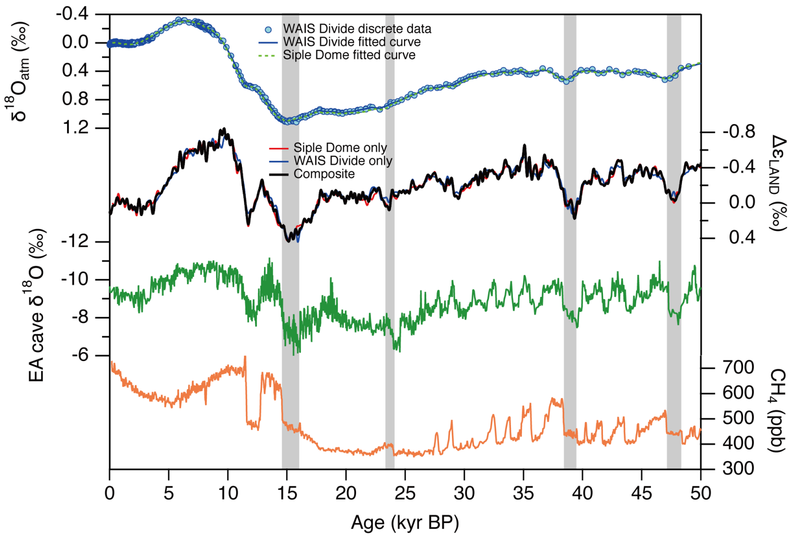

Figure 11: Atmospheric and hydrological records over the past 50 kyr: $\delta^{18}O_{atm}$ of the WAIS Divide core (Seltzer et al., 2017), $\Delta\varepsilon_{LAND}$ (terrestrial $\delta^{18}O$ fractionation), $\delta^{18}O$ of Southeast Asian speleothems (Cheng et al., 2016), and CH_4 concentrations from the WAIS Divide core (Rhodes et al., 2015). Grey shadings represent the periods of climate impact due to Heinrich events 1, 2, 4, and 5 as proposed by Rhodes et al. (2015) based on the CH_4 variations, which coincide with strong anomalies in $\Delta\varepsilon_{LAND}$ and speleothem $\delta^{18}O$ suggesting an anomalous southward shift of ITCZ.

$\delta^{18}O_{atm}$ as a dating tool

Because of its global-scale signature, the $\delta^{18}O_{atm}$ is also useful for ice core dating. A common way is orbital tuning, in which a $\delta^{18}O_{atm}$ record is matched to an orbital tuning target, e.g., precession parameter, insolation, or a mixture of precession and obliquity signals, with a constant phasing constrained at the last deglaciation (Shackleton, 2000). The phasings vary by several thousand years (Kawamura et al., 2007; Suwa and Bender, 2008a), which should be included in the uncertainty estimates (Bazin et al., 2013; Parrenin et al., 2001; Veres et al., 2013).

For the AICC2012 chronology (Veres et al., 2013; Bazin et al., 2013), a widely used chronology for four Antarctic ice cores (EDC, Vostok, TALDICE, and EDML), the $\delta^{18}O_{atm}$ records were matched to the 65˚N summer solstice insolation curve at every midpoint with the constant lag of 5.9 ± 6.0 kyr (Dreyfus et al., 2007; Suwa and Bender, 2008a). The AICC 2012 chronology around 110 kyr BP is markedly younger than the U-Th chronologies of speleothems and the Dome Fuji DF2021 chronology (mostly based on the O_2/N_2 age markers) (Extier et al., 2018; Oyabu et al., 2022; Veres et al., 2013), which is attributable to overestimation of the lag of $\delta^{18}O_{atm}$ behind insolation for ~100 – 120 kyr BP (Oyabu et al., 2022). The mean lag over the last 207 kyr is 4.1 ± 2.8 kyr (2 σ) according to the DF2021 chronology, which is smaller than that at the last deglaciation (~6 kyr).

The $\delta^{18}O_{atm}$ records can also be matched to the speleothem $\delta^{18}O$ records to employ their U-Th chronologies (currently, over the past 640 kyr) (Extier et al., 2018). Note that the uncertainty of resulting ice-core chronology mostly depends on that of the U-Th dating, which is less than ~1 kyr in the last interglacial period and becomes larger towards the older ages. The matching with speleothems also has the advantage of obtaining precise relative chronology of polar climate records with respect to the low- to mid-latitude climates.

Summary

-The elemental and isotopic ratios of N_2, O_2 and Ar in the ice cores provide various information on the past glaciological and climatological conditions as well as chronology.

-$\delta O_2/N_2$ and $\delta Ar/N_2$ reflect the fractionation during the bubble close-off and provide local summer insolation proxy at the coring site, which is useful as a dating tool for inland Antarctic deep ice cores.

-$\delta O_2/N_2$ also reveals long-term decreasing trend in atmospheric O_2 concentration over the last 800 kyr.

-$\delta^{15}N$ and $\delta^{40}Ar$ are gravitationally and thermally fractionated in firn by molecular diffusion, and they are used to reconstruct past firn thickness and surface temperature, including abrupt temperature changes.

-$\delta^{18}O_{atm}$ reflects the changes in terrestrial $\delta^{18}O$ fractionation and global oceanic $\delta^{18}O$, and it is used for investigating the low-latitude hydrological cycle as well as constraining chronologies.

-The $\delta O_2/N_2$, $\delta Ar/N_2$, $\delta^{18}O$ and $\delta^{40}Ar$ in ice cores may also be fractionated by artifactual gas loss after coring.

References

Barkan, E., Luz, B. (2005). High precision measurements of $^{17}O/^{16}O$ and $^{18}O/^{16}O$ ratios in H_2O. Rapid Commun. Mass Spectrom. 19, 3737-3742.

Battle, M., Bender, M., Sowers, T., Tans, P.P., Butler, J.H., Elkins, J.W., Ellis, J.T., Conway, T., Zhang, N., Lang, P., Clarke, A.D. (1996). Atmospheric gas concentrations over the past century measured in air from firn at the South Pole. Nature 383, 231-235.

Battle, M. O., Severinghaus, J. P., Sofen, E. D., Plotkin, D., Orsi, A. J., Aydin, M., Montzka, S. A., Sowers, T., Tans, P. P. (2011). Controls on the movement and composition of firn air at the West Antarctic Ice Sheet Divide. Atmos. Chem. Phys., 11(21), 11007–11021.

Bazin, L., Landais, A., Capron, E., Masson-Delmotte, V., Ritz, C., Picard, G., Jouzel, J., Dumont, M., Leuenberger, M., Prié, F. (2016). Phase relationships between orbital forcing and the composition of air trapped in Antarctic ice cores. Clim. Past 12, 729-748.

Bazin, L., Landais, A., Lemieux-Dudon, B., Toyé Mahamadou Kele, H., Veres, D., Parrenin, F., Martinerie, P., Ritz, C., Capron, E.F.N., Lipenkov, V., Loutre, M.F., Raynaud, D., Vinther, B., Svensson, A., Rasmussen, S.O., Severi, M., Blunier, T., Leuenberger, M., Fischer, H., Masson-Delmotte, V., Chappellaz, J., Wolff, E. (2013). An optimized multi-proxy, multi-site Antarctic ice and gas orbital chronology (AICC2012): 120-800 ka. Clim. Past 9, 1715-1731.

Bender, M., Sowers, T., Labeyrie, L. (1994). The Dole Effect and its variations during the last 130,000 years as measured in the Vostok Ice Core. Global Biogeochem. Cycles 8, 363-376.

Bender, M., Sowers, T., Lipenkov, V. (1995). On the concentrations of O_2, N_2, and Ar in trapped gases from ice cores. J. Geophys. Res. 100, 18651-18660.

Bender, M.L. (2002). Orbital tuning chronology for the Vostok climate record supported by trapped gas composition. Earth Planet. Sci. Lett 204, 275-289.

Berner, R.A. (2006). Geological nitrogen cycle and atmospheric N_2 over Phanerozoic time. Geol. 34, 413-415.

Bréant, C., Martinerie, P., Orsi, A., Arnaud, L., Landais, A. (2017). Modelling firn thickness evolution during the last deglaciation: constraints on sensitivity to temperature and impurities. Clim. Past 13, 833-853.

Buizert, C., Fudge, T.J., Roberts, W.H.G., Steig, E.J., Sherriff-Tadano, S., Ritz, C., Lefebvre, E., Edwards, J., Kawamura, K., Oyabu, I., Motoyama, H., Kahle, E.C., Jones, T.R., Abe-Ouchi, A., Obase, T., Martin, C., Corr, H., Severinghaus, J.P., Beaudette, R., Epifanio, J.A., Brook, E.J., Martin, K., Chappellaz, J., Aoki, S., Nakazawa, T., Sowers, T., Alley, R., Ahn, J., Sigl, M., Severi, M., Dunbar, N.W., Svensson, A., Fegyveresi, J., He, C., Liu, Z., Zhu, J., Otto-Bliesner, B., Lipenkov, V., Kageyama, M., Schwander, J. (2021). Antarctic-wide surface temperature and elevation during the Last Glacial Maximum. Science 372, 1097-1101.

Buizert, C., Gkinis, V., Severinghaus, J.P., He, F., Lecavalier, B.S., Kindler, P., Leuenberger, M., Carlson, A.E., Vinther, B., Masson-Delmotte, V., White, J.W.C., Liu, Z., Otto-Bliesner, B., Brook, E.J. (2014). Greenland temperature response to climate forcing during the last deglaciation. Science 345, 1177-1180.

Buizert, C., Martinerie, P., Petrenko, V.V., Severinghaus, J.P., Trudinger, C.M., Witrant, E., Rosen, J.L., Orsi, A.J., Rubino, M., Etheridge, D.M., Steele, L.P., Hogan, C., Laube, J.C., Sturges, W.T., Levchenko, V.A., Smith, A.M., Levin, I., Conway, T.J., Dlugokencky, E.J., Lang, P.M., Kawamura, K., Jenk, T.M., White, J.W.C., Sowers, T., Schwander, J., Blunier, T. (2012). Gas transport in firn: multiple-tracer characterisation and model intercomparison for NEEM, Northern Greenland. Atmos. Chem. Phys. 12, 4259-4277.

Cheng, H., Edwards, R.L., Sinha, A., Spötl, C., Yi, L., Chen, S., Kelly, M., Kathayat, G., Wang, X., Li, X., Kong, X., Wang, Y., Ning, Y., Zhang, H. (2016). The Asian monsoon over the past 640,000 years and ice age terminations. Nature 534, 640-646.

Craig, H., Horibe, Y., Sowers, T. (1988). Gravitational separation of gases and isotopes in polar ice caps. Science 23, 1675-1678.

Dole, M. (1935). The relative atomic weight of oxygen in water and in air. J. Am. Chem. Soc. 57, 2731.

Dreyfus, G.B., Parrenin, F., Lemieux-Dudon, B., Durand, G., Masson-Delmotte, V., Jouzel, J., Barnola, J.M., Panno, L., Spahni, R., Tisserand, A., Siegenthaler, U., Leuenberger, M. (2007). Anomalous flow below 2700 m in the EPICA Dome C ice core detected using $\delta^{18}O$ of atmospheric oxygen measurements. Clim. Past 3, 341-353.
Extier, T., Landais, A., Bréant, C., Prié, F., Bazin, L., Dreyfus, G., Roche, D.M., Leuenberger, M. (2018). On the use of $\delta^{18}O_{atm}$ for ice core dating. Quat. Sci. Rev. 185, 244-257.
Fujita, S., Okuyama, J., Hori, A., Hondoh, T. (2009). Metamorphism of stratified firn at Dome Fuji, Antarctica: A mechanism for local insolation modulation of gas transport conditions during bubble close off. J. Geophys. Res. 114.
Grachev, A.M., Severinghaus, J.P. (2003a). Determining the Thermal Diffusion Factor for $^{40}Ar/^{36}Ar$ in Air To Aid Paleoreconstruction of Abrupt Climate Change. J. Phys. Chem. A 107, 4636-4642.
Grachev, A.M., Severinghaus, J.P. (2003b). Laboratory determination of thermal diffusion constants for $^{29}N_2/^{28}N_2$ in air at temperatures from -60 to 0°C for reconstruction of magnitudes of abrupt climate changes using the ice core fossil-air paleothermometer. Geochim. Cosmochim. Acta 67, 345-360.
Helman, Y., Barkan, E., Eisenstadt, D., Luz, B., Kaplan, A. (2005). Fractionation of the three stable oxygen isotopes by oxygen-producing and oxygen-consuming reactions in photosynthetic organisms. Plant Physiol. 138, 2292-2298.
Horibe, Y., Shigehara, K., Langway Jr, C.C. (1985). Chemical and isotopic composition of air inclusions in a Greenland ice core. Earth Planet. Sci. Lett 73, 207-210.
Huang, E., Wang, P., Wang, Y., Yan, M., Tian, J., Li, S., Ma, W. (2020). Dole effect as a measurement of the low-latitude hydrological cycle over the past 800 ka. Sci. Adv. 6, 2375-2548.
Huber, C., Beyerle, U., Leuenberger, M., Schwander, J., Kipfer, R., Spahni, R., Severinghaus, J.P., Weiler, K. (2006a). Evidence for molecular size dependent gas fractionation in firn air derived from noble gases, oxygen, and nitrogen measurements. Earth Planet. Sci. Lett 243, 61-73.
Huber, C., Leuenberger, M., Spahni, R., Flückiger, J., Schwander, J., Stocker, T.F., Johnsen, S., Landais, A., Jouzel, J. (2006b). Isotope calibrated Greenland temperature record over Marine Isotope Stage 3 and its relation to CH_4. Earth Planet. Sci. Lett 243, 504-519.
Hutterli, M., Schneebeli, M., Freitag, J., Kipfstuhl, J., Röthlisberger, R. (2009). Impact of local insolation on snow metamorphism and ice core records. Physics of Ice Core Records II : Papers collected after the 2nd International Workshop on Physics of Ice Core Records, held in Sapporo, Japan, 2-6 February 2007. Edited by Takeo Hondoh.
Ikeda, T., Fukazawa, H., Mae, S., Pepin, L., Duval, P., Champagnon, B., Lipenkov, V. Y., Hondoh, T. (1999). Extreme fractionation of gases caused by formation of clathrate hydrates in Vostok Antarctic ice. Geophysical Research Letters, 26(1), 91–94.
Ikeda-Fukazawa, T., Fukumizu, K., Kawamura, K., Aoki, S., Nakazawa, T., Hondoh, T. (2005). Effects of molecular diffusion on trapped gas composition in polar ice cores. Earth Planet. Sci. Lett 229, 183-192.
Ikeda-Fukazawa, T., Hondoh, T., Fukumura, T., Fukazawa, H., Mae, S. (2001). Variation in N_2/O_2 ratio of occluded air in Dome Fuji antarctic ice. J. Geophys. Res. 106, 17799-17810.
Ikeda-Fukazawa, T., Kawamura, K., Hondoh, T. (2004). Diffusion of nitrogen gas in ice Ih. Chemical Physics Letters 385, 467-471.
Jouzel, J., Hoffmann, G., Parrenin, F., Waelbroeck, C. (2002). Atmospheric oxygen 18 and sea-level changes. Quat. Sci. Rev. 21, 307-314.
Jouzel, J., Masson-Delmotte, V., Cattani, O., Dreyfus, G., Falourd, S., Hoffmann, G., Minster, B., Nouet, J., Barnola, J.M., Chappellaz, J., Fischer, H., Gallet, J.C., Johnsen, S., Leuenberger, M., Loulergue, L., Luethi, D., Oerter, H., Parrenin, F., Raisbeck, G., Raynaud, D., Schilt, A., Schwander, J., Selmo, E., Souchez, R., Spahni, R., Stauffer, B., Steffensen, J.P., Stenni, B., Stocker, T.F., Tison, J.L., Werner, M., Wolff, E.W. (2007). Orbital and Millennial Antarctic Climate Variability over the Past 800,000 Years. Science 317, 793-796.

Kawamura, K., Parrenin, F., Lisiecki, L., Uemura, R., Vimeux, F., Severinghaus, J.P., Hutterli, M.A., Nakazawa, T., Aoki, S., Jouzel, J., Raymo, M.E., Matsumoto, K., Nakata, H., Motoyama, H., Fujita, S., Goto-Azuma, K., Fujii, Y., Watanabe, O. (2007). Northern Hemisphere forcing of climatic cycles in Antarctica over the past 360,000years. Nature 448, 912-916.

Kawamura, K., Severinghaus, J.P., Albert, M.R., Courville, Z.R., Fahnestock, M.A., Scambos, T., Shields, E., Shuman, C.A. (2013). Kinetic fractionation of gases by deep air convection in polar firn. Atmos. Chem. Phys. 13, 11141-11155.

Kawamura, K., Severinghaus, J.P., Ishidoya, S., Sugawara, S., Hashida, G., Motoyama, H., Fujii, Y., Aoki, S., Nakazawa, T. (2006). Convective mixing of air in firn at four polar sites. Earth Planet. Sci. Lett 244, 672-682.

Kobashi, T., Severinghaus, J.P., Barnola, J.-M. (2008a). 4±1.5 °C abrupt warming 11,270 yr ago identified from trapped air in Greenland ice. Earth Planet. Sci. Lett 268, 397-407.

Kobashi, T., Severinghaus, J.P., Kawamura, K. (2008b). Argon and nitrogen isotopes of trapped air in the GISP2 ice core during the Holocene epoch (0–1,500 B.P.): Methodology and implications for gas loss processes. Geochim. Cosmochim. Acta 72, 4675-4686.

Landais, A., Barnola, J.M., Kawamura, K., Caillon, N., Delmotte, M., van Ommen, T., Dreyfus, G., Jouzel, J., Masson-Delmotte, V., Minster, B., Freitag, J., Leuenberger, M., Schwander, J., HUBER, C., Etheridge, D., Morgan, V. (2006). Firn-air $\delta^{15}N$ in modern polar sites and glacial–interglacial ice: a model-data mismatch during glacial periods in Antarctica? Quat. Sci. Rev. 25, 49-62.

Landais, A., Caillon, N., Goujon, C., Grachev, A.M., Barnola, J.M., Chappellaz, J., Jouzel, J., Masson-Delmotte, V., Leuenberger, D. (2004). Quantification of rapid temperature change during DO event 12 and phasing with methane inferred from air isotopic measurements. Earth Planet. Sci. Lett 225, 221-232.

Landais, A., Dreyfus, G., Capron, E., Masson-Delmotte, V., Sanchez-GoNi, M.F., Desprat, S., Hoffmann, G., Jouzel, J., Leuenberger, M., Johnsen, S. (2010). What drives the millennial and orbital variations of $\delta^{18}O_{atm}$? Quat. Sci. Rev. 29, 235-246.

Landais, A., Dreyfus, G., Capron, E., Pol, K., Loutre, M.F., Raynaud, D., Lipenkov, V.Y., Arnaud, L., Masson-Delmotte, V., Paillard, D., Jouzel, J., Leuenberger, M. (2012). Towards orbital dating of the EPICA Dome C ice core using $\delta O_2/N_2$. Clim. Past 8, 191-203.

Landais, A., Masson-Delmotte, V., Combourieu Nebout, N., Jouzel, J., Blunier, T., Leuenberger, M., Dahl-Jensen, D., Johnsen, S. (2007). Millenial scale variations of the isotopic composition of atmospheric oxygen over Marine Isotopic Stage 4. Earth Planet. Sci. Lett 258, 101-113.

Lang, C., Leuenberger, M., Schwander, J., Johnsen, S. (1999). 16˚C rapid temperature variation in central Greenland 70,000 years ago Science 286, 934-937.

Lüthi, D., Bereiter, B., Stauffer, B., Winkler, R., Schwander, J., Kindler, P., Leuenberger, M., Kipfstuhl, J., Capron, E., Landais, A., Fischer, H., Stocker, T.F. (2010). CO_2 and O_2/N_2 variations in and just below the bubble–clathrate transformation zone of Antarctic ice cores. Earth Planet. Sci. Lett 297, 226-233.

Luz, B., Barkan, E. (2011). The isotopic composition of atmospheric oxygen. Global Biogeochem. Cycles 25.

Markle, B.R., Steig, E.J. (2022). Improving temperature reconstructions from ice-core water-isotope records. Clim. Past 18, 1321-1368.

Morgan, J.D., Buizert, C., Fudge, T.J., Kawamura, K., Severinghaus, J.P., Trudinger, C.M. (2022). Gas isotope thermometry in the South Pole and Dome Fuji ice cores provides evidence for seasonal rectification of ice core gas records. The Cryosphere 16, 2947-2966.

Morita, N. (1935). The increased density of air oxygen relative to water oxygen. Journal of the Chemical Society of Japan 56.

Ohno, H., Lipenkov, V.Y., Hondoh, T. (2010). Formation of air clathrate hydrates in polar ice sheets: heterogeneous nucleation induced by micro-inclusions. J. Glaciol. 56, 917-921.

Oppo, D.W., Lehman, S. (1995). Suborbital timescale variability of North Atlantic Deep Water during the past 200,000 years. Paleoceanography and Paleoclimatology 10, 901-910.

Orsi, A.J., Cornuelle, B.D., Severinghaus, J.P. (2014). Magnitude and temporal evolution of Dansgaard–Oeschger event 8 abrupt temperature change inferred from nitrogen and argon isotopes in GISP2 ice using a new least-squares inversion. Earth Planet. Sci. Lett 395, 81-90.

Oyabu, I., Kawamura, K., Buizert, C., Parrenin, F., Orsi, A., Kitamura, K., Aoki, S., Nakazawa, T. (2022). The Dome Fuji ice core DF2021 chronology (0-207 kyr BP). Quat. Sci. Rev. 294.

Oyabu, I., Kawamura, K., Kitamura, K., Dallmayr, R., Kitamura, A., Sawada, C., Severinghaus, J.P., Beaudette, R., Orsi, A., Sugawara, S., Ishidoya, S., Dahl-Jensen, D., Goto-Azuma, K., Aoki, S., Nakazawa, T. (2020). New technique for high-precision, simultaneous measurements of CH_4, N_2O and CO_2 concentrations, isotopic and elemental ratios of N_2, O_2 and Ar, and total air content in ice cores by wet extraction. Atmos. Meas. Tech. 13, 6703-6731.

Oyabu, I., Kawamura, K., Uchida, T., Fujita, S., Kitamura, K., Hirabayashi, M., Aoki, S., Morimoto, S., Nakazawa, T., Severinghaus, J.P., Morgan, J. (2021). Fractionation of O_2/N_2 and Ar/N_2 in the Antarctic ice sheet during bubble formation and bubble–clathrate hydrate transition from precise gas measurements of the Dome Fuji ice core. The Cryosphere 15, 5529-5555.

Parrenin, F., Barker, S., Blunier, T., Chappellaz, J., Jouzel, J., Landais, A., Masson-Delmotte, V., Schwander, J., Veres, D. (2012). On the gas-ice depth difference (Δdepth) along the EPICA Dome C ice core. Clim. Past 8, 1239-1255.

Parrenin, F., Jouzel, J., Waelbroeck, C., Ritz, C., Barnola, J.-M. (2001). Dating the Vostok ice core by an inverse method. J. Geophys. Res.: Atmospheres 106, 31837-31851.

Paterson, W.S.B. (1969). The physics of glaciers (Pergamon, Oxford).

Reutenauer, C., Landais, A., Blunier, T., Bréant, C., Kageyama, M., Woillez, M.N., Risi, C., Mariotti, V., Braconnot, P. (2015). Quantifying molecular oxygen isotope variations during a Heinrich stadial. Clim. Past 11, 1527-1551.

Rhodes, R.H., Brook, E.J., Chiang, J.C.H., Blunier, T. (2015). Enhanced tropical methane production in response to iceberg discharge in the North Atlantic. Science 348, 1016-1019.

Salamatin, A.N., Lipenkov, V., Ikeda-Fukazawa, T., Hondoh, T. (2001). Kinetics of air-hydrate nucleation in polar ice sheets. J. Cryst. Growth 223, 285-305.

Schwander, J., Sowers, T., Barnola, J.M., Blunier, T., Fuchs, A., Malaize, B. (1997). Age scale of the air in the summit ice: Implication for glacial-interglacial temperature change. J. Geophys. Res.: Atmospheres 102, 19483-19493.

Seltzer, A.M., Buizert, C., Baggenstos, D., Brook, E.J., Ahn, J., Yang, J.-W., Severinghaus, J.P. (2017). Does $\delta^{18}O$ of O_2 record meridional shifts in tropical rainfall? Clim. Past 13, 1323-1338.

Severinghaus, J.P., Albert, M.R., Courville, Z.R., Fahnestock, M.A., Kawamura, K., Montzka, S.A., Mühle, J., Scambos, T.A., Shields, E., Shuman, C.A., Suwa, M., Tans, P., Weiss, R.F. (2010). Deep air convection in the firn at a zero-accumulation site, central Antarctica. Earth Planet. Sci. Lett 293, 359-367.

Severinghaus, J. P., Grachev, A., Battle, M. (2001). Thermal fractionation of air in polar firn by seasonal temperature gradients. Geochemistry Geophysics Geosystems, 2(7), 1048–24.

Severinghaus, J.P. and Battle, M.O. (2006). Fractionation of gases in polar ice during bubble close-off: New constraints from firn air Ne, Kr and Xe observations. Earth Planet. Sci. Lett 244, 474-500.

Severinghaus, J.P., Beaudette, R., Headly, M.A., Taylor, K., Brook, E.J. (2009). Oxygen-18 of O_2 Records the Impact of Abrupt Climate Change on the Terrestrial Biosphere. Science 324, 1431-1434.

Severinghaus, J.P., Brook, E. (1999). Abrupt climate change at the end of the last glacial period Inferred from trapped air in polar Ice. Science 286, 930-934.

Severinghaus, J.P., Grachev, A., Luz, B., Caillon, N. (2003). A method for precise measurement of argon 40/36 and krypton/argon ratios in trapped air in polar ice with applications to past firn thickness and abrupt climate change in Greenland and at Siple Dome, Antarctica. Geochim. Cosmochim. Acta 67, 325-343.

Severinghaus, J.P., Sowers, T., Brook, E., Alley, R.B., Bender, M. (1998). Timing of abrupt climate change at the end of the Younger Dryas interval from thermally fractionated gases in polar ice. Nature 391, 141-146.

Shackleton, N.J. (2000). The 100,000-Year Ice-Age Cycle Identified and Found to Lag Temperature, Carbon Dioxide, and Orbital Eccentricity. Science 289, 1897-1902.

Shackleton, S., Bereiter, B., Baggenstos, D., Bauska, T.K., Brook, E.J., Marcott, S.A., Severinghaus, J.P. (2019). Is the Noble Gas-Based Rate of Ocean Warming During the Younger Dryas Overestimated? Geophys. Res. Lett. 46, 5928-5936.

Sowers, T., Bender, M., Raynaud, D. (1989). Elemental and isotopic composition of occluded O_2 and N_2 in polar ice. J. Geophys. Res. 94, 5137-5150.

Sowers, T., Bender, M., Raynaud, D., Korotkevich, Y.S. (1992). $\delta^{15}N$ of N_2 in air trapped in polar ice: A tracer of gas transport in the firn and a possible constraint on ice age ‐ gas age differences. J. Geophys. Res. 97, 15683-15697.

Stolper, D.A., Bender, M.L., Dreyfus, G.B., Yan, Y., Higgins, J.A. (2016). A Pleistocene ice core record of atmospheric O_2 concentrations. Science 353, 1427-1430.

Suwa, M., Bender, M.L. (2008a). Chronology of the Vostok ice core constrained by O_2/N_2 ratios of occluded air, and its implication for the Vostok climate records. Quat. Sci. Rev. 27, 1093-1106.

Suwa, M., Bender, M.L. (2008b). O_2/N_2 ratios of occluded air in the GISP2 ice core. J. Geophys. Res.: Atmospheres 113.

Uchida, T., Yasuda, K., Oto, Y., Shen, R., Ohmura, R. (2014). Natural supersaturation conditions needed for nucleation of air-clathrate hydrates in deep ice sheets. J. Glaciol. 60, 1111-1116.

Uemura, R., Motoyama, H., Masson-Delmotte, V., Jouzel, J., Kawamura, K., Goto-Azuma, K., Fujita, S., Kuramoto, T., Hirabayashi, M., Miyake, T., Ohno, H., Fujita, K., Abe-Ouchi, A., Iizuka, Y., Horikawa, S., Igarashi, M., Suzuki, K., Suzuki, T., Fujii, Y. (2018). Asynchrony between Antarctic temperature and CO2 associated with obliquity over the past 720,000 years. Nat. Commun 9.

Veres, D., Bazin, L., Landais, A., Toyé Mahamadou Kele, H., Lemieux-Dudon, B., Parrenin, F., Martinerie, P., Blayo, E., Blunier, T., Capron, E., Chappellaz, J., Rasmussen, S.O., Severi, M., Svensson, A., Vinther, B., Wolff, E.W. (2013). The Antarctic ice core chronology (AICC2012): an optimized multi-parameter and multi-site dating approach for the last 120 thousand years. Clim. Past 9, 1733-1748.

Yan, Y., Brook, E.J., Kurbatov, A.V., Severinghaus, J.P., Higgins, J.A. (2021). Ice core evidence for atmospheric oxygen decline since the Mid-Pleistocene transition. Sci. Adv. 7.